Uppermost mantle (Pn) velocity model for the Afar region, Ethiopia: An insight into rifting processes

Geophysical Journal International

Geophys. J. Int. (2013) **193,** 321–328 doi: 10.1093/gji/ggs106

Uppermost mantle (P_n) velocity model for the Afar region, Ethiopia: an insight into rifting processes

A. L. Stork,[1,*] G. W. Stuart,[1] C. M. Henderson,[2,†] D. Keir[3] and J. O. S. Hammond[4,§]

[1]*Institute of Geophysics and Tectonics, School of Earth and Environment, University of Leeds, Leeds,* LS2 9JT*, UK. E-mail: anna.stork@bristol.ac.uk*
[2]*School of Geography, Environmental and Earth Sciences, Victoria University of Wellington, P.O. Box* 600*, Wellington, New Zealand*
[3]*National Oceanography Centre Southampton, University of Southampton, Southampton,* SO14 3ZH*, UK*
[4]*School of Earth Sciences, University of Bristol, Bristol* BS8 1RJ*, UK*

Accepted 2012 December 11. Received 2012 December 10; in original form 2012 September 17

SUMMARY

The Afar Depression, Ethiopia, offers unique opportunities to study the transition from continental rifting to oceanic spreading because the process is occurring onland. Using traveltime tomography and data from a temporary seismic deployment, we describe the first regional study of uppermost mantle *P*-wave velocities (V_{Pn}). We find two separate low V_{Pn} zones (as low as 7.2 km s^{-1}) beneath regions of localized thinned crust in northern Afar, indicating the existence of high temperatures and, potentially, partial melt. The zones are beneath and off-axis from, contemporary crustal magma intrusions in active magmatic segments, the Dabbahu-Manda-Hararo and Erta'Ale segments. This suggests that these intrusions can be fed by off-axis delivery of melt in the uppermost mantle and that discrete areas of mantle upwelling and partial melting, thought to characterize segmentation of the uppermost mantle at seafloor spreading centres, are initiated during the final stages of break-up.

Key words: Seismicity and tectonics; Seismic tomography; Continental margins: divergent.

1 INTRODUCTION

In the basic model of continental rifting a region undergoes extension during which the crust and upper mantle are stretched and thinned (McKenzie 1978). This results in the upwelling of hotter mantle material, causing partial melting, intrusion into the continental lithosphere and, eventually, the creation of new oceanic crust (e.g. Hayward & Ebinger 1996). Early models of magmatism at plate-spreading centres assumed symmetric rifting about the rift axis (e.g. Buck & Su 1989) and observations suggested the presence of narrow zones of melt beneath the axis (Detrick *et al.* 1987; Macdonald & Fox 1988).

The mantle response to lithospheric thinning and intrusion during continental break-up remains poorly understood. The Afar Depression, Ethiopia, offers a unique opportunity to address this problem because it subaerially exposes the transition from break-up to spreading. We describe the first regional study of uppermost mantle *P*-wave velocities (V_{Pn}) from a recent temporary seismic deployment in Afar (e.g. Belachew *et al.* 2011). Low *P*-wave velocity zones indicate high temperatures and melt anomalies, placing constraints on the geometry of uppermost mantle upwelling during the transition from continental to oceanic rifting.

The Afar Depression, covering parts of Ethiopia, Djibouti and Eritrea (see Fig. 1), is a ∼300 km wide region that has developed during rifting between Africa and Arabia over ∼30 Myr (Wolfenden *et al.* 2005). The centre of the rift-rift-rift triple junction between the Red Sea Rift, the Gulf of Aden Rift and the Main Ethiopian Rift (MER) is currently located around 11°N 42°E on the Ethiopian/Djibouti border (Fig. 1). Magmatic intrusion is playing an important role in accommodating strain during rifting in Ethiopia, evidenced by dyke intrusion episodes along an ∼80-km-long section of the Dabbahu-Manda-Hararo (DMH) segment of the Red Sea Rift since 2005 September (Wright *et al.* 2006, 2012; Grandin *et al.* 2010b).

The depression exhibits some features of model rift zones including crustal thinning (45–15 km, e.g. Hammond *et al.* 2011a) and relatively low seismic velocities in the upper mantle with rapid changes in upper mantle velocities over short distances (50–100 km) reported beneath both the MER and the Afar Depression (Bastow *et al.* 2008). Bastow & Keir (2011) argue that the thinning of the crust in northernmost Afar indicates the final stages of break-up, with stretching and thinning of the heavily intruded and weakened plate promoting decompression melting of the mantle. Afar has also been described as a nascent oceanic rift (e.g. Rowland *et al.* 2007) because individual rift segments have spatial and structural characteristics in common with slow-spreading mid-ocean ridges

∗Now at: School of Earth Sciences, University of Bristol, Bristol BS8 1RJ, UK.
†Now at: GLOBE Claritas, GNS Science, 1 Fairway Drive, Avalon 5010, PO Box 30-368, Lower Hutt 5040, New Zealand.
§Now at: Department of Earth Science and Engineering, South Kensington Campus, Imperial College, London, SW7 2AZ, UK.

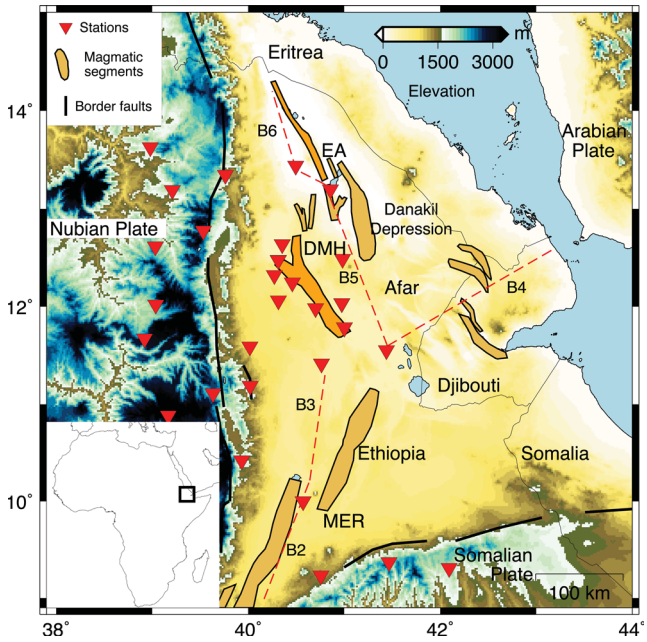

Figure 1. Map showing the location (see inset) and topography of the Afar region with areas of Quaternary-Recent volcanism, labelled as magmatic segments (Wright *et al.* 2012). The Dabbahu-Manda-Hararo (DMH) and Erta'Ale (EA) magmatic segments are labelled and highlighted. The locations of the seismic stations used in this study are also given. The seismic refraction profiles of Berckhemer *et al.* (1975) are indicated by the dashed red lines. MER is the Main Ethiopian Rift.

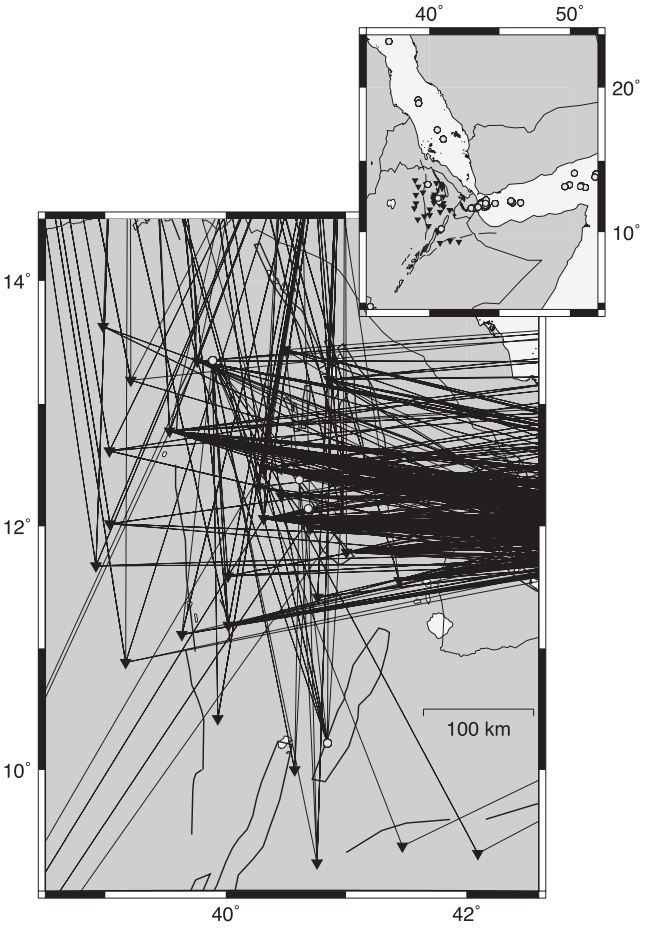

Figure 2. Ray path coverage from the earthquakes meeting the selection criteria. Inverted triangles represent the seismic stations. The circles indicate the earthquake epicentres in the inset figure.

(Hayward & Ebinger 1996). The spreading rate in the Depression is also similar to slow-spreading ridges (6–20 mm yr^{-1}; McClusky *et al.* 2010; Kogan *et al.* 2012).

The theoretical description of P_n is a refracted wave at the Moho and the first earthquake arrival at regional distances (~100–1600 km). Therefore, P_n tomographic studies can be used to study the physical characteristics of the Earth at the Moho and in the uppermost mantle (e.g. Bannister *et al.* 1991; Hearn & Ni 1994). A global review found that continental settings have an average V_{Pn} of 8.1 km s^{-1} (Christensen & Mooney 1995), whereas mid-ocean ridges have V_{Pn} as low as 7.2 km s^{-1} (e.g. Dunn *et al.* 2005). These velocities provide constraints on changes in temperature, pressure and composition (e.g. Perry *et al.* 2006) and the spatial distribution of mantle upwelling and partial melt (e.g. Dunn *et al.* 2001). Here, we use the tomographic inversion method of Seward *et al.* (2009) to determine the spatial variation in V_{Pn} beneath the Afar Depression using relative P_n arrival times between pairs of stations.

2 DATA SELECTION

Absolute P_n first arrivals are picked from bandpass filtered (0.5–5.0 Hz) vertical component seismograms recorded at 50 samples/s on temporary SEIS-UK and IRIS-PASSCAL broad-band seismometer networks deployed in Afar between 2007 January and 2010 December (Fig. 1; Belachew *et al.* 2011). Data from regional earthquakes, at distances 200–1500 km from the stations (Fig. 2), are used in this study. The selected minimum source–station distance of 200 km is the estimated minimum distance to ensure the waves are sampling the uppermost mantle. Controlled source and passive seismic experiments in the Afar Depression, where the crust is ~15–30 km thick, indicate that a minimum source-station distance at which P_n will be observed is 70–110 km (Makris & Ginzburg 1987). On the western plateau flanks of the rift the crust is up to 45 km thick (e.g. Dugda *et al.* 2007; Hammond *et al.* 2011a) producing an estimated minimum distance for P_n observations of 200 km. At such distances in southern Afar, the rays used in this study are likely to be sampling below the velocity discontinuity described by Makris & Ginzburg (1987) at ~40 km depth and not the Moho depth determined by these authors and Hammond *et al.* (2011a). In northern Afar no significant velocity discontinuity below the Moho is observed by Makris & Ginzburg (1987) and at 200 km distance the observations provide information from diving waves at ~30 km depth in the uppermost mantle (Makris & Ginzburg 1987).

Crustal earthquakes with magnitudes ≥4.0 and with epicentres estimated using arrivals at a minimum of five stations with a maximum azimuthal gap of 230° are chosen from the National Earthquake Information Center catalogue to ensure the epicentres are well determined. These selection criteria result in a total of 612 manually determined arrival times at 33 stations from 65 earthquakes. Fig. 2 shows the ray path coverage.

The relative arrival times between pairs of stations used in the tomographic inversion are limited to those at similar azimuths from the epicentre using

$$\left(\Delta_j - \Delta_i\right) \geq \Delta_{ij} \cos 35^\circ.$$

This is comparable to the criteria used by Haines (1979), where $\Delta_{i,j}$ is the source–station distance to station i or station j and $\Delta_{i,j}$ is

the distance from station i to j, and it ensures that the ray paths to each station pair are similar while still providing a good number of relative times to conduct the inversion.

3 P_n TRAVELTIME TOMOGRAPHY

In this study, we use the V_{Pn} tomographic modelling method that is described in detail in Seward *et al.* (2009).

The method uses least-squares collocation (Moritz 1972) and relative arrival times at pairs of stations (Haines 1979) and forms a simple model of the form:

$$\mathbf{Mp} = \boldsymbol{\ell} + \mathbf{E}. \tag{1}$$

In eq. (1), **M** is the design matrix and contains a mathematical description of the deterministic part of the model; **p** contains the modelling parameters; $\boldsymbol{\ell}$ is the vector of observations of traveltime differences between stations; and **E** is a combination of measurement uncertainties in the arrival times and the probabilistic component of the model for the mantle and crust. The inversion is performed as a normal weighted least squares inverse:

$$\underline{\hat{p}} = \left[\mathbf{M}^T\mathbf{C}_{\text{tot}}^{-1}\mathbf{M}\right]^{-1}\mathbf{M}^T\mathbf{C}_{\text{tot}}^{-1}l, \tag{2}$$

$$\mathbf{C}_{\text{tot}} = \text{cov}(\mathbf{E}). \tag{3}$$

The result of eq. (2) is $\underline{\hat{p}}$, which is simply the average slowness. The residuals can then be calculated from the parameter estimate and the design matrix. The estimation of the slowness surface is derived from the residual vector as follows:

$$\text{s} = \mathbf{C}_{\text{sl}}\mathbf{C}_{\text{tot}}^{-1}\mathbf{r}. \tag{4}$$

In eq. (4), **s** is a signal (see Moritz 1972), **r** is the vector of residuals and $\mathbf{C}_{\text{sl}}$ is the covariance between the signal-points and the observation. The form of matrix $\mathbf{C}_{\text{sl}}$ is dependent on which signal is being calculated, e.g. mantle *P*-wave slowness or crustal delay.

This method has advantages over parametrized gridded methods (e.g. Rawlinson *et al.* 2001) because:

(1) Prior knowledge and constraints on structural variability can be introduced. These parameters guide the model but do not place rigid constraints on the calculation and they can be overcome by the data (Seward *et al.* 2009).

(2) The inverse problem is always over determined because the average slowness is the only parameter to be determined. A limited number of suitable earthquakes are available for this study and therefore an inversion using a gridded method could be unstable.

(3) Explicit estimates for the uncertainties, combining both measurement and modelling uncertainties, can be made for any location, even those far from any discrete data.

The formation of $\mathbf{C}_{\text{tot}}$ combines estimates of measurement errors in P_n arrival times and of the correlation of the slowness between any two points in the crust or mantle (Seward *et al.* 2009). The measurement error is estimated as 0.25 s, based on a study of the analyst's ability to pick first arrival times (Stork 2007). Mantle and crustal covariances are calculated using correlation distances defined for the crust and mantle. Previous studies (e.g. Bastow *et al.* 2008; Hammond *et al.* 2011b) have shown that the dominant wavelengths of features in the upper mantle are on the order of 100 km and checkerboard tests suggest a mantle correlation distance of 100 km is a good compromise between resolution and noise for features >100 km in wavelength (Fig. 3). The correlation distance in the crust is estimated to be about 10 km because studies in Afar have shown that crustal thicknesses and velocities vary over such distances (e.g. Hammond *et al.* 2011a).

A 1.5 s maximum station delay term is also input to the model, to account for variations in crustal thickness and velocity structure below stations. This is estimated by applying Snell's law, assuming critical refraction of P_n at the crust mantle boundary, an average crustal velocity of 6.25 km s^{-1} (Makris & Ginzburg 1987) and a change in crustal thickness of 5 km over 10 km laterally (Hammond *et al.* 2011a).

Because our velocity model is calculated from relative arrival times, the influence of errors in earthquake hypocentres and origin times is minimized. Even so, estimates of the epicentre uncertainty are included in the model calculation. We use an estimated epicentre uncertainty of 15 km because errors of this magnitude are typically reported for global catalogues (e.g. Engdahl *et al.* 1998). All the earthquakes are reported to occur <13 km deep in the crust and are therefore suitable for sampling the uppermost mantle.

The implemented criteria resulted in the use of 500 relative arrival times to compute the V_{Pn} model and the calculation is performed as a weighted least-squares inversion. As described above, the output from the classical inversion process is a single parameter, the average slowness. However, using the methods of least squares collocation, the residuals from this inversion can then be used to estimate the stochastic components of the model. These estimates will be mathematical descriptions of the best estimates for the continuous surfaces that describe V_{Pn}, crustal terms and, just as importantly, the uncertainties in these surfaces.

4 RESULTS

4.1 V_{Pn} model for Afar, Ethiopia

The estimated V_{Pn} model for the Afar region and the associated standard deviations are presented in Fig. 4. The model is dominated by two very low-velocity zones, one with V_{Pn} as low as 7.2 km s^{-1}, located beneath and to the west of the active DMH rift segment. The standard deviation is 0.2–0.3 km s^{-1} in the majority of this area. The other low V_{Pn} area is located to the northwest of Erta'Ale volcano and has a velocity of 7.2 $\pm$ 0.4 km s^{-1}. The most recent tectonic activity in the area includes inferred dyke intrusions into the DMH segment (e.g. Grandin *et al.* 2010a; Belachew *et al.* 2011) and recent eruptions of Erta'Ale (e.g. Field *et al.* 2012) and Alu-Dalafilla (Pagli *et al.* 2012) volcanoes, both on the Erta'Ale segment. The low-velocity zones cover an area broader than the mapped segments and extend over ~100 km laterally.

At the edges of the two zones the velocity changes rapidly over ~50 km to normal continental V_{Pn} (defined by Christensen & Mooney (1995) as being 8.0–8.2 km s^{-1}) and mostly normal continental V_{Pn} are observed in the remainder of the region (within the errors in the model), see Fig. 4. An exception to this general picture appears to be low V_{Pn} (~7.6 km s^{-1}) on the flanks of the western plateau (beneath and south of stations BTIE and DERE, Fig. 4). This finding is in agreement with studies suggesting that hot partially molten material exists towards the edge of the rift (e.g. Keir *et al.* 2009; Guidarelli *et al.* 2011; Hammond *et al.* 2011a; Rychert *et al.* 2012), although the estimated errors do not completely rule out velocities up to 8.0 km s^{-1}.

For comparison with our V_{Pn} results, Fig. 4 also illustrates the upper mantle velocities found by Makris & Ginzburg (1987) with the profiles labelled B3, B4, B5 and B6. The overall pattern and values for uppermost mantle velocities presented here are consistent

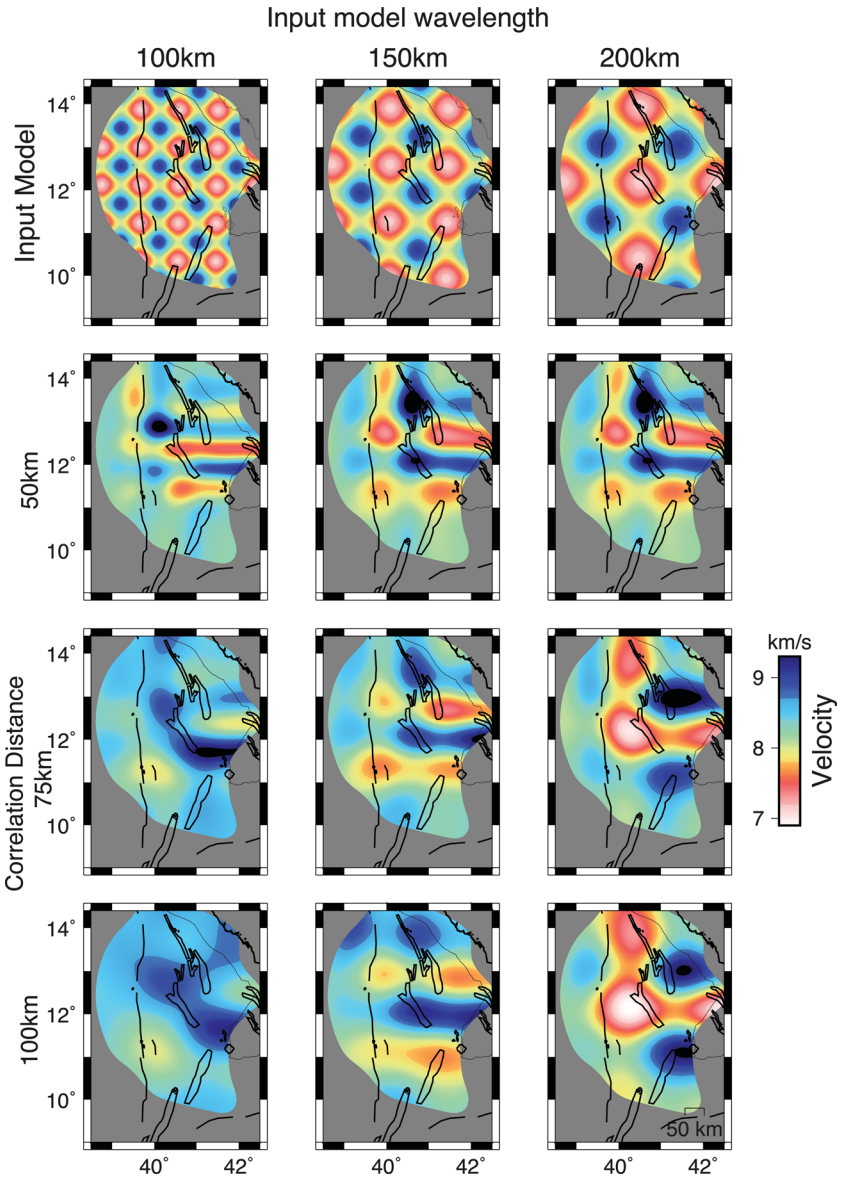

Figure 3. Modelling resolution test. The synthetic checkerboard input velocity models with wavelengths of 100 km, 150 km and 200 km are shown on the top row. Below are the computed velocity models for these inputs using mantle correlation distances of 50, 75 and 100 km and the available traveltimes. The border faults and magmatic segments are highlighted, as in Fig. 1. The area displayed is that shown for the results in Fig. 4.

with these 2-D refraction models. Both studies find low velocities below active magmatic segments (profiles B5 and B6) and normal mantle velocities elsewhere in the region (profiles B3 and B4). At the northern end of profile B5 Makris & Ginzburg (1987) report P velocities of 7.8 km s^{-1} at depths ∼30 km. This is in agreement with the velocities reported here between the two low-velocity zones. The standard deviations in V_{Pn} between the two low-velocity zones (0.3–0.4 km s^{-1}) in this study suggest it is unlikely, but possible, that the two low V_{Pn} areas are connected. It is also possible that the uppermost few km of the mantle are not sampled by the rays because the Moho shallows rapidly to the north in this area (Makris & Ginzburg 1987). Therefore lower velocities than the 7.8 km s^{-1} reported could exist in shallowest few km of the mantle.

Nabro volcano, close to the Eritrean/Ethiopian border (13.37°N, 41.70°E), was active in 2011 but we report normal continental velocities (∼8.0 km s^{-1}) below the volcano. This could be because there is poor crossing ray coverage in this area (Fig. 2) and the standard deviation in the estimated P_n velocity is $>\pm 0.4$ km s^{-1} (Fig. 4); or because the volcano is fed by a small (< 50 km wide) and distinct magmatic zone that is not resolved by the data (see Section 4.2).

4.2 Effect of model resolution on interpretation

Following the inversion, the tomographic model resolution is also tested to determine the results from certain configurations of low-velocity zones in the uppermost mantle. We use input V_{Pn} models with a normal continental V_{Pn} (8.0 km s^{-1}) background, and a slowness perturbation of ±0.015 s/km is used to produce low-velocity zones with V_{Pn} as low as 7.1 km s^{-1}. The same input parameters and traveltime data are used as for the results in Fig. 4. We have chosen to present the results of three synthetic models using low-velocity zones at various locations and with various sizes (Fig. 5). Fig. 5(c) best matches the data inversion and has 150-km-wide low-velocity zones in the uppermost mantle beneath and offset from the DMH segment and EA segment (Fig. 4). The first two models

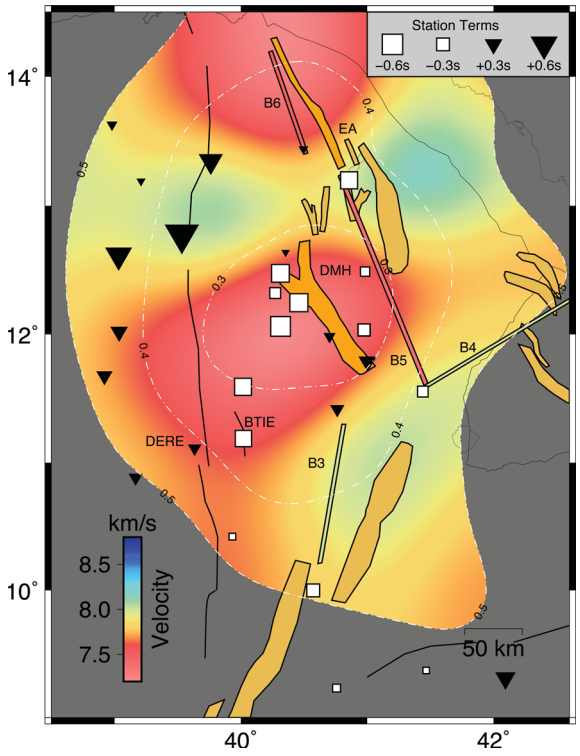

Figure 4. Computed V_{Pn} model describing lateral velocity variations for the Afar region with low velocities indicated by red colours. The grey shaded area has a standard deviation, σ, in the velocity of $>\pm 0.5\,\mathrm{km\,s^{-1}}$. The $\sigma = 0.3\,\mathrm{km\,s^{-1}}$ and $0.4\,\mathrm{km\,s^{-1}}$ contours are also indicated by the white dashed lines. The stations used to estimate the model are shown by black triangles (with positive station delay terms) and white squares (with negative station terms). The upper mantle velocities estimated by Makris & Ginzburg (1987) on lines B3, B4, B5 and B6 are indicated in the relevant colours on the map.

show 50-km- and 100-km-wide low-velocity zones (Figs 5a and b, respectively) placed directly below recent eruption sites (Dabbahu, Manda-Hararo, Erta'Ale and Nabro). However, as stated in the previous section, we are unable to properly resolve the smaller features (if they exist), particularly in the Nabro area where there is no ray coverage. In our subsequent interpretation of the results we discuss the features we are able resolve, with wavelengths >100 km and in areas with standard deviations in velocity of $<0.5\,\mathrm{km\,s^{-1}}$.

4.3 Station delays

Station delay terms are also estimated in the inversion. These terms reflect relative differences in crustal thicknesses and velocities between stations (Seward *et al.* 2009). As expected, Fig. 4 shows that stations on the plateaux in Ethiopia, where the crust is thickest, have positive station terms and stations with negative terms are situated in the rift where the crust has been found to be thin (e.g. Hammond *et al.* 2011a).

5 DISCUSSION

The pattern of low V_{Pn} observed in this study help to constrain continent-to-ocean transition rift models. Such models predict that lithospheric thinning and mantle upwelling during rifting produce thermal anomalies, adiabatic decompression of the mantle and sometimes partial melting (McKenzie & Bickle 1988).

The pattern of low V_{Pn} zones reported here indicates that discrete areas of high temperatures, and likely partial melting, exist in the uppermost mantle beneath the Afar Depression. This provides new evidence that present day focussed magmatic crustal intrusions and active magmatism, reported by geophysical studies of the area (Grandin *et al.* 2010a; Guidarelli *et al.* 2011; Hammond *et al.* 2011a), are fed by concurrent and distinct thermal anomalies in the uppermost mantle that are surrounded by higher velocity regions with *P*-wave velocities approaching those expected for the uppermost mantle in continental settings (7.8–$8.0\,\mathrm{km\,s^{-1}}$). This observation is also consistent with mantle tomography results showing similar localized features $\sim$50 km in wavelength at shallow depths ($\sim$75 km) in the upper mantle (Hammond *et al.* 2011b). Similar findings have been reported by Wang *et al.* (2009), who observe focussed upper mantle upwellings beneath the Gulf of California oblique rift, comparable in separation and size to the low V_{Pn} zones observed in this study. In addition, Ligi *et al.* (2012) report that isolated areas of oceanic crust, separated by 50–100 km, developed in the Red Sea at the inception of seafloor spreading. These studies suggest that the segmentation is because of dynamic upwelling driven by melt buoyancy effects or the reduced density of depleted mantle and that it is influenced by structures pre-existing continental break-up. Ligi *et al.* (2012) argue that, in the Red Sea, the lower continental lithosphere was replaced by upwelling asthenosphere before the initiation of continental rupture. In this particular study, we cannot rule out that the low-velocity zones are caused by partial melt that is initially intruded into thinned continental lithosphere.

Wang *et al.* (2009) also find some off-axis low velocities in the Gulf of California, as we do in this study. The low V_{Pn} zones beneath Afar extend from directly below the magmatic segments (DMH and Erta'Ale) to up to 75 km laterally to one side (Fig. 4), suggesting that crustal intrusions in Afar may originate from on- and off-axis melt in the uppermost mantle. At the western edge of the DMH low-velocity zone, below the flanks of the western plateau, the crust is >30 km thick and we find velocities around $7.6\,\mathrm{km\,s^{-1}}$. Another possibility for these off-axis low velocities west of the DMH segment is that this signature is a remnant of earlier rifting and magmatic activity. A similar signature has also been observed in the results of previous crust and mantle studies (Guidarelli *et al.* 2011; Hammond *et al.* 2011a; Rychert *et al.* 2012). Tesfaye *et al.* (2003) suggest the triple junction developed around 10 Ma at 10°N 40–41°E and the area has undergone successive rifting episodes since then with the triple junction moving $\sim$160 km northeast. Volcanism <3 Ma has been reported in the area where we find low velocities (11°–12°N, 40–41°E; e.g. Lahitte *et al.* 2003). Low *P*-wave velocities could be because of ongoing magmatism and partial melt in the uppermost mantle. This has previously been suggested as the explanation for low velocities (Keir *et al.* 2009) and hot material (Whaler & Hautot 2006) in the lower crust and upper mantle observed below the flanks of the western plateau.

Lithospheric thinning during the late stages of continental break-up promotes the formation of decompression melting that feeds dyke intrusions. Comparing our V_{Pn} results with estimates of crustal thickness (Makris & Ginzburg 1987; Hammond *et al.* 2011a), the lowest velocities are observed in distinct localized areas of Afar where the crust has been stretched and thinned to <25 km beneath and adjacent to active magmatic segments. This suggests that the delivery of melt to the uppermost mantle is coincident with lithospheric thinning and deeper mantle anomalies.

The spreading rate in Afar is similar to slow-spreading mid-ocean ridges (15–20 mm $\mathrm{yr^{-1}}$, e.g. Kogan *et al.* 2012). Slow-spreading mid-ocean ridge studies predict that melt flux is focused in the

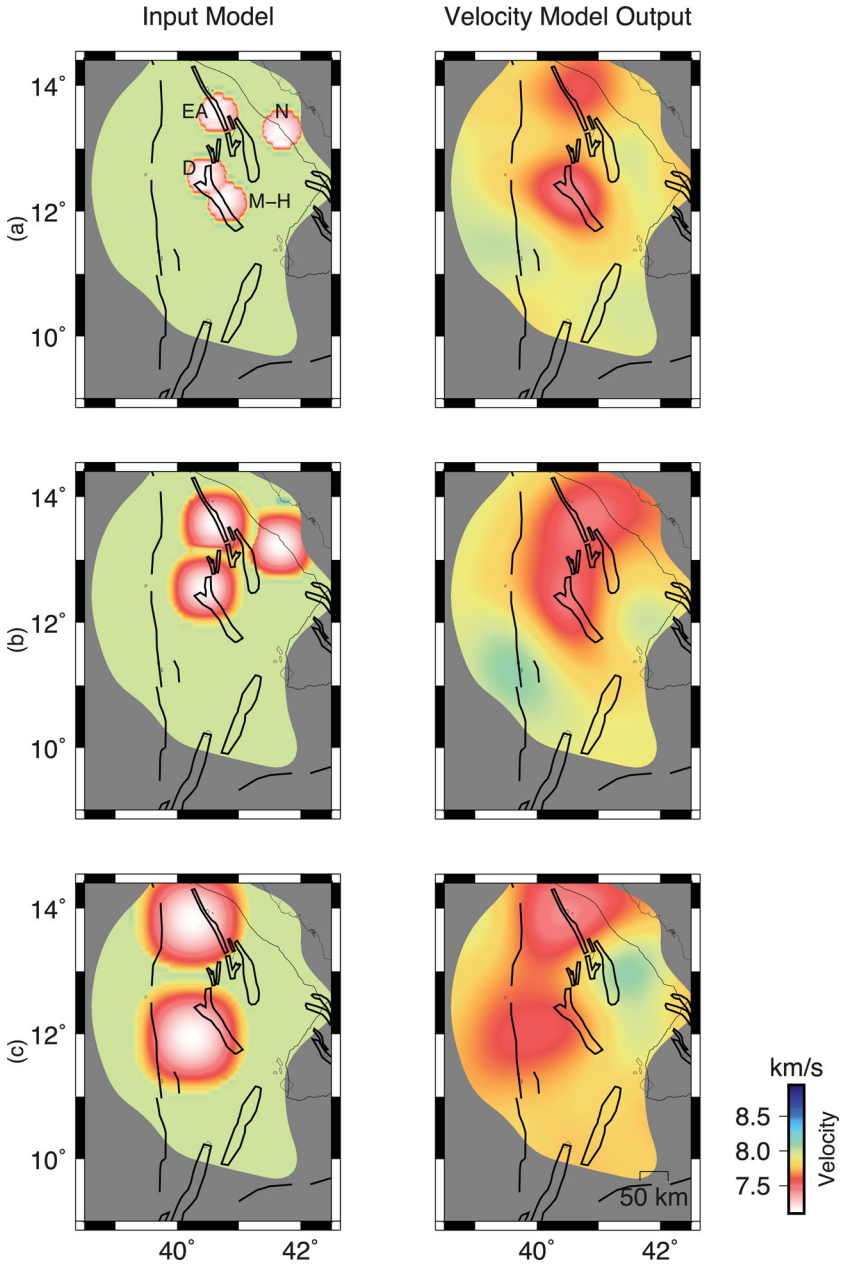

Figure 5. Model resolution tests using synthetic input velocity models (left). V_{Pn} model outputs are computed using the available ray coverage and shown on the right. The border faults and magmatic segments are highlighted, as in Fig. 1. (a) An input model with 50 km diameter low V_{Pn} below Dabbahu (D), Manda-Hararo (M-H), Erta'Ale (EA) and Nabro (N) volcanoes. (b) An input with 100 km diameter low V_{Pn} below D, EA and N volcanoes. (c) An input model with 150 km anomalies offset from DMH and EA segments.

mantle and then delivered to a segment centre (e.g. Whitehead *et al.* 1984; Lin *et al.* 1990) and seismic experiments at the slow-spreading Mid-Atlantic Ridge find low-velocity zones extending from the lower crust to the upper mantle that are consistent with high temperatures and the presence of melt (Canales *et al.* 2000; Dunn *et al.* 2005). Surface and crustal observations in Afar have shown that the magmatic segments have structural and spatial characteristics in common with slow-spreading mid-ocean ridge segments (e.g. Hayward & Ebinger 1996). For the first time, we report uppermost mantle velocities during continental break-up similar in character to the segmentation observed at slow-spreading mid-ocean ridges (e.g. Dunn *et al.* 2005) and the Gulf of California oblique rift (Wang *et al.* 2009).

Laboratory experiments suggest that changes in the uppermost mantle velocity of up to 6 per cent can be explained by thermal anomalies alone, without a need for partial melt (e.g. Sato *et al.* 1988). Mantle anisotropy, caused by crystal alignment along strain axes, and melt geometry are also likely to affect travel-times in the Afar region (e.g. Kendall 2000). Previous shear-wave anisotropy studies of the MER and Afar show a fast direction parallel to the rift axis (Kendall *et al.* 2005; Keir *et al.* 2011). Because the majority of regional earthquakes recorded by the temporary seismic deployments occur to the north and east of the network (only one earthquake occurred to the southwest, Fig. 2) it is not possible to make a measurement of anisotropy in this study.

In this study reductions in V_{Pn} of 12 per cent from normal P_n velocities are observed but the amount of melt in the uppermost mantle is difficult to estimate. It is unlikely that anisotropy could fully explain the two dramatic low-velocity zones observed here because P_n anisotropy studies report maximum amplitudes resulting in 7.5 per cent changes in velocity (e.g. Hearn 1996; Pei *et al.* 2007). Through analytical experiments Hammond & Humphreys (2000) demonstrate a reduction in V_{Pn} of at least 3.6 per cent in velocity per 1 per cent in partial melt, suggesting that partial melt of around 3 per cent could be present beneath the active segments in Afar.

6 CONCLUSION

This study is the first regional study of uppermost mantle velocities (V_{Pn}) in the Afar Depression, Ethiopia. Using traveltime tomographic inversion, we find two very low V_{Pn} zones below and near to the active DMH and Erta'Ale magmatic rift segments. In these areas V_{Pn} is as low as $7.2 \pm 0.2\,\mathrm{km\,s^{-1}}$, providing evidence that the present day crustal intrusions and surface activity are fed by localized and on- and off-axis areas of decompression melting in the uppermost mantle. These low V_{Pn} zones coincide with areas of stretched and thinned crust, suggesting that decompression melting is caused by ongoing mechanical deformation of the plate, as well as removal of melt from the mantle. Our observations indicate that discrete zones of upwelling, thought to characterize segmentation of the uppermost mantle at ocean ridges, initiate during the late stages of continental rifting.

ACKNOWLEDGMENTS

We thank two anonymous reviewers and Kathy Whaler for their constructive comments on the manuscript. The project was supported by grants from NERC (NE/E007414/1) and NSF (EAR-0635789). ALS and JOSH acknowledge support from the NERC grant. The equipment was loaned from NERC Seis-UK and IRIS-PASSCAL. Cindy Ebinger is acknowledged for providing access to the NSF data. We thank Atalay Ayele and staff at the IGSSA Addis Ababa University for their scientific and logistical contribution; and the Afar National Regional State Government for field support.

REFERENCES

Bannister, S.C., Ruud, B.O. & Husebye, E.S., 1991. Tomographic estimates of sub-Moho seismic velocities in Fennoscandia and structural implications, *Tectonophysics,* **189,** 37–53.

Bastow, I.D. & Keir, D., 2011. The protracted development of the continent-ocean transition in Afar, *Nat. Geosci.,* **4,** 248–250.

Bastow, I.D., Nyblade, A.A., Stuart, G.W., Rooney, T.O. & Benoit, M.H., 2008. Upper mantle seismic structure beneath the Ethiopian hot spot: rifting at the edge of the African low-velocity anomaly, *Geochem. Geophys. Geosysts.,* **9,** Q12022, doi:10.1029/2008GC002107.

Belachew, M., Ebinger, C., Cote, D., Keir, D., Rowland, J.V., Hammond, J.O.S. & Ayele, A., 2011. Comparison of dike intrusions in an incipient seafloor-spreading segment in Afar, Ethiopia: seismicity perspectives, *J. geophys. Res.,* **116,** B06405, doi:10.1029/2010JB007908.

Berckhemer, H. *et al.*, 1975. Deep seismic soundings in the Afar region and on the highland of Ethiopia, in *Afar depression of Ethiopia: Proceedings of the international symposium on the Afar region and related rift problems, held in Bad Bergzabern, FR Germany, 1–6 April, 1974,* pp. 89–107, Schweizerbart, Stuttgart.

Buck, W.R. & Su, W., 1989. Focused mantle upwelling below mid-ocean ridges due to feedback between viscosity and melting, *Geophys. Res. Lett.,* **16,** 641–644.

Canales, J.P., Collins, J.A., Escartin, J. & Detrick, R.S., 2000. Seismic structure across the rift valley of the Mid-Atlantic Ridge at 23°20′ (MARK area): implications for crustal accretion processes at slow spreading ridges, *J. geophys. Res.,* **105,** 28 411–28 425.

Christensen, N.I. & Mooney, W.D., 1995. Seismic velocity structure and composition of the continental crust: a global view, *J. geophys. Res.,* **100,** 9761–9788.

Detrick, R.S., Buhl, P., Vera, E., Mutter, J., Orcutt, J., Madsen, J. & Brocher, T., 1987. Multi-channel seismic imaging of a crustal magma chamber along the East Pacific Rise, *Nature,* **326,** 35–41.

Dugda, M.T., Nyblade, A.A. & Jordi, J., 2007. Thin lithosphere beneath the Ethiopian plateau revealed by a joint inversion of Rayleigh wave group velocities and receiver functions, *J. geophys. Res.,* **112,** B08305, doi:10.1029/2006JB004918.

Dunn, R.A., Toomey, D.R., Detrick, R.S. & Wilcock, W.S.D., 2001. Continuous mantle melt supply beneath an overlapping spreading center on the East Pacific Rise, *Science,* **291,** 1955–1958.

Dunn, R.A., Lekic, V., Detrick, R.S. & Toomey, D.R., 2005. Three-dimensional seismic structure of the Mid-Atlantic Ridge (35°N): evidence for focused melt supply and lower crustal dike injection, *J. geophys. Res.,* **110,** B09101, doi:10.1029/2004JB003473.

Engdahl, E.R., van der Hilst, R. & Buland, R., 1998. Global teleseismic earthquake relocation with improved travel times and procedures for depth determination, *Bull. seism. Soc. Am.,* **88,** 722–743.

Field, L., Barnie, T., Blundy, J., Brooker, R.A., Keir, D., Lewi, E. & Saunders, K., 2012. Integrated field, satellite and petrological observations of the November 2010 eruption of Erta Ale, *Bull. Volcanol.,* **74,** 2251–2271.

Grandin, R., Socquet, A., Doin, M.-P., Jacques, E., de Chabalier, J.B. & King, G.C.P., 2010a. Transient rift opening in response to multiple dike injections in the Manda Hararo rift (Afar, Ethiopia) imaged by time-dependent elastic inversion of interferometric synthetic aperture radar data, *J. geophys. Res.,* **115,** B09403, doi:10.1029/2009JB006883.

Grandin, R., Socquet, A., Jacques, E., Mazzoni, N., De Chabalier, J.B. & King, G.C.P., 2010b. Sequence of rift- ing in Afar (Manda-Hararo rift, Ethiopia, 2005–2009): time-space evolution and interactions between dikes from InSAR and static stress change modeling, *J. geophys. Res.,* **115,** B10413, doi:10.1029/2009JB000815.

Guidarelli, M., Stuart, G., Hammond, J.O.S., Kendall, J.M., Ayele, A. & Belachew, M., 2011. Surface wave tomography across Afar, Ethiopia: crustal structure at a rift triple-junction zone, *Geophys. Res. Lett.,* **38,** L24313, doi:10.1029/2011GL046840.

Haines, A.J., 1979. Seismic-wave velocities in the uppermost mantle beneath New Zealand, *N.Z. J. Geol. Geophys.,* **22,** 242–257.

Hammond, J.O.S, Kendall, J.-M., Stuart, G.W., Keir, D., Ebinger, C., Ayele, A. & Belachew, M., 2011a. The nature of the crust beneath the Afar triple junction: evidence from receiver functions, *Geochem. Geophys. Geosysts.,* **12,** Q12004, doi:10.1029/2011GC003738.

Hammond, J.O.S. *et al.*, 2011b. Seismically imaging the Afar plume, American Geophysical Union, Fall Meeting 2011, Abstract #DI13A-2155.

Hammond, W.C. & Humphreys, E.D., 2000. Upper mantle seismic wave velocity: effects of realistic partial melt geometries, *J. geophys. Res.,* **105,** 10 975–10 986.

Hayward, N.J. & Ebinger, C.J., 1996. Variations in the along-axis segmentation of the Afar Rift system, *Tectonics,* **15,** 244–257.

Hearn, T.M., 1996. Anisotropic P_n tomography in the western United States, *J. geophys. Res.,* **101,** 8403–8414.

Hearn, T.M. & Ni, J.F., 1994. P_n velocities beneath continental collision zones–the Turkish-Iranian plateau, *Geophys. J. Int.,* **117,** 273–283.

Keir, D., Bastow, I.D., Whaler, K.A., Daly, E., Cornwell, D.G. & Hautot, S., 2009. Lower crustal earthquakes near the Ethiopian rift induced by magmatic processes, *Geochem. Geophys. Geosysts.,* **10,** Q0AB02, doi:10.1029/2009GC2382.

Keir, D., Belachew, M., Ebinger, C.J., Kendall, J.M., Hammond, J.O.S., Stuart, G.W., Ayele, A. & Rowland, J.V., 2011. Mapping the evolving strain field during continental breakup from

crustal anisotropy in the Afar Depression, *Nature Comms.,* **2,** 285, doi:10.1038/ncomms1287.

Kendall, J.M., 2000. Seismic anisotropy in the boundary layers of the mantle, in *Earth's Deep Interior: Mineral Physics and Tomography From the Atomic to the Global Scale,* Vol. 117, pp. 133–159, eds Karato, S., Forte, A.M., Liebermann, R.C., Masters, G. & Stixrude, L., Geophysical Monograph, AGU, Washington DC.

Kendall, J.M., Stuart, G.W., Ebinger, C.J., Bastow, I.D. & Keir, D., 2005. Magma-assisted rifting in Ethiopia, *Nature,* **433,** 146–148.

Kogan, L., Fisseha, S., Bendick, R., Reilinger, R., McClusky, S., King, R. & Solomon, T., 2012. Lithospheric strength and strain localization in continental extension from observations of the East African Rift, *J. geophys. Res.,* **117,** B03402, doi:10.1029/2011JB008516.

Lahitte, P., Gillot, P.-Y., Kidane, T., Courtillot, V. & Bekele, A., 2003. New age constraints on the timing of volcanism in central Afar, in the presence of propagating rifts, *J. geophys. Res.,* **108**(B2), 2123, doi:10.1029/2001JB001689.

Ligi, M. *et al.*, 2012. Birth of an ocean in the Red Sea: initial pangs, *Geochem. Geophys. Geosysts.,* **13,** Q08009, doi:10.1029/2012GC004155.

Lin, J., Purdy, G.M., Schouten, H., Sempere, J.C. & Zervas, C., 1990. Evidence from gravity-data for focused magmatic accretion along the Mid-Atlantic Ridge, *Nature,* **6267,** 627–632.

Macdonald, K.C. & Fox, P.J., 1988. The axial summit graben and cross-sectional shape of the East Pacific Rise as indicators of axial magma chambers and recent volcanic eruptions, *Earth planet. Sci. Lett.,* **88,** 119–131.

Makris, J. & Ginzburg, A., 1987. The Afar depression—transition between continental rifting and sea-floor spreading, *Tectonophysics,* **141,** 199–214.

McClusky, S. *et al.*, 2010. Kinematics of the southern Red Sea-Afar Triple Junction and implications for plate dynamics, *Geophys. Res. Lett.,* **37,** L05301, doi:10.1029/2009GL041127.

McKenzie, D., 1978. Some remarks on the development of sedimentary basins, *Earth planet. Sci. Lett.,* **40,** 25–32.

McKenzie, D. & Bickle, M.J., 1988. The volume and composition of melt generated by extension of the lithosphere, *J. Petrol.,* **29,** 625–679.

Moritz, H., 1972. *Advanced Least-Squares Methods,* Dep. of Geod. Sci., Ohio State Univ., Ohio.

Pagli, C., Wright, T.J., Ebinger, C.J., Yun, S.-H., Cann, J.R., Barnie, T. & Ayele, A., 2012. Shallow axial magma chamber at the slow-spreading Erta Ale Ridge, *Nat. Geosci.,* **5,** 284–288.

Pei, S.P. *et al.*, 2007. Upper mantle seismic velocities and anisotropy in China determined through P_n and S_n tomography, *J. geophys. Res.,* **112,** B05312, doi:10.1029/2006JB004409.

Perry, H.K.C., Jaupart, C., Mareschal, J.C. & Shapiro, N.M., 2006. Upper mantle velocity-temperature conversion and composition determined from seismic refraction and heat flow, *J. geophys. Res.,* **111,** B07301, doi:10.1029/2005JB003921.

Rawlinson, N., Houseman, G.A. & Collins, C.D.N., 2001. Inversion of seismic refraction and wide-angle reflection traveltimes for three-dimensional layered structure, *Geophys. J. Int.,* **145,** 381–400.

Rowland, J.V., Baker, E., Ebinger, C.J., Keir, D., Kidane, T., Biggs, J., Hayward, N. & Wright, T.J., 2007. Fault growth at a nascent slow-spreading ridge: 2005 Dabbahu rifting episode, Afar, *Geophys. J. Int.,* **171,** doi:10.1111/j.1365-246X.2007.03584.x.

Rychert, C.A. *et al.*, 2012. Volcanism in the Afar Rift sustained by decompression melting with minimal plume influence, *Nat. Geosci.,* **5,** 406–409.

Sato, H., Sacks, I.S., Murase, T. & Scarfe, C.M., 1988. Thermal structure of the low velocity zone derived from laboratory and seismic investigations, *Geophys. Res. Lett.,* **15,** 1227–1230.

Seward, A.M., Henderson, C.M. & Smith, E.G.C., 2009. Models of the upper mantle beneath the central North Island, New Zealand, from speeds and anisotropy of subhorizontal *P* waves (P_n), *J. geophys. Res.,* **114,** B0131, doi:10.1029/2008JB005805.

Stork, A.L., 2007. Optimisation and application of earthquake location methods, *D.Phil. thesis,* Univ. of Oxford, UK.

Tesfaye, S., Harding, D.J. & Kusky, T.M., 2003. Early continental breakup boundary and migration of the Afar triple junction, Ethiopia, *Geol. Soc. Am. Bull.,* **115,** 1053–1067.

Wang, Y., Forsyth, D.W. & Savage, B., 2009. Convective upwelling in the mantle beneath the Gulf of California, *Nature,* **462,** 499–501.

Whaler, K.A. & Hautot, S., 2006. The electrical resistivity structure of the crust beneath the northern Main Ethiopian Rift, in *The Afar Volcanic Province within the East African Rift System,* Vol. 259, pp. 55–72, eds Yirgu, G., Ebinger, C.J. & Maguire, P.K.H., Geol. Soc. London Spec. Publ., doi:10.1144/GSL.SP.2006.259.01.22.

Whitehead, J.A., Dick, H.J.B. & Schouten, H., 1984. A mechanism for magmatic accretion under spreading centres, *Nature,* **312,** 146–148.

Wolfenden, E., Ebinger, C., Yirgu, G., Renne, P.R. & Kelley, S.P., 2005. Evolution of a volcanic rifted margin: Southern Red Sea, Ethiopia, *Geol. Soc. Am. Bull.,* **117,** 846–864.

Wright, T.J., Ebinger, C., Biggs, J., Ayele, A., Yirgu, G., Keir, D. & Stork, A., 2006. Magma-maintained rift segmentation at continental rupture in the 2005 Afar dyking episode, *Nature,* **442,** 291–294.

Wright, T.J. *et al.*, 2012. Geophysical constraints on the dynamics of spreading centres from rifting episodes on land, *Nat. Geosci.,* **5,** 242–250.